

**SIXTH EUROPEAN ROTORCRAFT AND
POWERED LIFT AIRCRAFT FORUM**

Paper No. 29

**RECENT PROGRESS IN
PERFORMANCE PREDICTION OF
HIGH ADVANCE RATIO
CIRCULATION CONTROLLED ROTORS**

Ernest O. Rogers
David W. Taylor Naval Ship Research and Development Center
Bethesda, Maryland, USA

September 16-19, 1980
Bristol, England

THE UNIVERSITY, BRISTOL, BS8 1HR, ENGLAND

RECENT PROGRESS IN PERFORMANCE PREDICTION OF HIGH ADVANCE RATIO CIRCULATION CONTROLLED ROTORS

Ernest O. Rogers
David W. Taylor Naval Ship Research and Development Center
Bethesda, Maryland, USA

ABSTRACT

The application of circulation control technology to rotors adds several new aerodynamic parameters to the design process and will permit expanded operating regimes for rotorcraft. High advance ratio (0.5 to 0.7) lifting rotor operation is characterized by highly nonuniform blade loading distributions, wake skew angles within a few degrees of the plane of rotation, and strong blade/vortex encounters. The development and validation of analytical procedures for the above conditions are essential to fully exploit advanced concepts such as the X-Wing VTOL aircraft. Accordingly, an extensive subscale rotor data base was used to develop a new, high advance ratio performance methodology. One major factor in the success achieved so far has been the use of a vortex wake inflow computer code. At all advance ratios examined (0.3 to 0.7), correct prediction of experimental roll moment and thrust resulted only when the vortex-based inflow theory was used. With the inflow field represented in this manner, the extensive circulation control airfoil data base, corrected appropriately for local flow conditions, can be applied in a classical quasi-steady blade element approach to rotor performance prediction. In related experimental investigations, flow visualization (tufts) at 0.7 advance ratio, has confirmed the suppression of separated flow by simultaneous leading and trailing edge blowing on the retreating side. The potential of higher harmonic pneumatic control has also been demonstrated by the virtual elimination of the twice-per-revolution blade flatwise moment.

1. INTRODUCTION

The application of circulation control (CC) airfoils to helicopter rotors presents an opportunity to greatly expand both speed and range-payload performance. References 1-5 describe design concepts which, in conjunction with thrust compounding, encompass a range of design advance ratios from 0.50 to infinity (stopped rotor) with corresponding maximum speeds from 200 to more than 500 knots. Figure 1 illustrates the various operating regimes of the X-Wing stopped rotor concept developed at the David W. Taylor Naval Ship Research and Development Center (DTNSRDC). Hover and low speed helicopter mode flight employ trailing edge blowing with cyclic modulation to provide control. Above an advance ratio of 0.5, simultaneous leading and trailing edge boundary layer control ("dual blowing") is employed on the retreating side to maintain lift in the reverse flow circle. Conversion to the fixed wing mode is initiated in the advance ratio range of 0.55 to 0.70. The rotor rotational rate is rapidly reduced to zero, thereby traversing all advance ratios from 0.55 to infinity. Fixed wing flight is then controlled using single slot blowing. The critical design conditions for the X-Wing rotor and blowing system occur in the vicinity of 0.7 advance ratio. In this operating regime, the rotor lifting capability and roll control margin reach a minimum. Unfortunately, the aerodynamic environment associated with this critical flight condition is extremely severe. As a consequence, the ultimate success of the X-Wing and other high speed rotor concepts depends heavily on the capability to optimize rotor performance in the previously unexplored high advance ratio *lifting rotor* range.

To address this outstanding problem, an extensive experimental and analytical program has been conducted at DTNSRDC over the past several years. More than 2000 wind tunnel occupancy hours have been accrued on a 7-foot diameter subscale model rotor. A large range of operating conditions and pneumatic control system parameters have been explored using this model with the results firmly establishing aerodynamic feasibility. Also during May 1979, a 25-foot flight worthy X-Wing rotor was successfully tested in the NASA Ames 40-foot X 80-foot wind tunnel. This test (Reference 6) further validated the aerodynamic performance expectations at high advance ratio, as well as closed loop control and structural goals. Even though an extensive

data base has been acquired, a validated high speed performance prediction capability is essential before efficient, "optimized," full scale vehicles can be designed and flown. The unusually large number of rotor design parameters (Table 1) demonstrates the importance of an analytic capability. A related use of the analysis is the physical insight provided into the detailed aerodynamic phenomena involved which may also influence the design selection. For these reasons, DTNSRDC has continued to develop and evaluate analytical procedures for calculation of CC rotor aerodynamics. Reference 7 details prior analytical development for low advance ratio CC rotors. This paper will address the analytical/physical complications of high advance ratio (0.4 to 0.7) operation and trace the evolution of analytical methods that have led to the successful correlation of experiment and theory.

2. MODEL ROTOR DESCRIPTION AND DATA BASE

The experimental data used in the correlation was obtained from wind tunnel evaluation of the subscale Reverse Blowing Circulation Control Rotor (RBCCR). This 6.7-foot diameter rotor (Figure 2) has untapered, untwisted aluminum blades with a fixed slot height of 0.002 chord. The first flap frequency is normally 2.3 per revolution (2.3p) making it a "rigid" rotor which, in fact, is representative of full scale design. No cyclic pitch mechanism is provided, nor is one needed. The collective angle can be manually adjusted by means of slotted bolt holes in the blade root flanges. Blade sections are symmetrical about the mid-chord, giving an aerodynamic profile independent of flow direction with separate ducts to supply air to the two identical slots.

Blade airfoil profile is a linear interpolation between specified root and tip cross sections. The tip airfoil was derived from a 15 percent ellipse by slightly rounding the leading/trailing edge to enhance Coanda sheet turning, while still providing satisfactory operation as a leading edge. A thickness of 15 percent was found to offer the highest critical Mach number in the outboard angle-of-attack operating range. The root section, a cambered 20 percent ellipse, was based on the most efficient two-dimensional section previously evaluated.

Most wind tunnel data was acquired at a constant tip speed of 250 feet per second due to tunnel velocity limitations. Corresponding blade internal pressure levels ranged from 2 to 5 pounds per square inch. The early tunnel entries used a cam/nozzle type of azimuthal pressure modulation scheme. The range of pressure waveforms (azimuthal thrust distribution) was limited. Later entries utilized an eight segment valve concept thereby providing greater control waveform freedom. The pressure measuring and recording system was also improved at this time, especially in regard to minimizing temperature effects on the duct pressure transducers. This set of data which covers the 0 to 5 degree shaft angle range was used for the final analysis-correlation effort. Figure 3 presents some of the wind tunnel results in terms of rotor system power required as a function of speed at zero shaft angle. Peak power coefficient is seen to occur at 0.7 advance ratio, as had been expected from the preliminary design studies. Having confirmed 0.7 as the critical speed, subsequent data acquisition and analysis concentrated on this flight condition. The very significant effects of shaft angle and cyclic control waveform on reducing power requirements were established experimentally. The objective was then to develop analysis methods that would correlate with the experimental results thereby validating a means of examining the effect of rotor design and operating parameters.

3. ANALYTICAL MODELING

3.1 General Approach

A classical blade element strip integration theory is used in the analysis with unique provisions for CC airfoil characteristics. Sections of the blade are considered as segments of an infinite aspect ratio wing with values of their aerodynamic coefficients based on steady state two-dimensional results modified for yawed flow phenomena. Blade end effects are approximated using root cutout and a tip lift loss factor. (The assumption of a root cutout would have to be modified with a lift carryover estimate when using the integrated hub fairings now being incorporated into the X-Wing design.) Inflow field determination requires an analysis method that can model the essential characteristics of the unique operating environment existing at high advance ratio. The validity of applying steady state circulation control results directly to the highly unsteady rotor environment has not been fully established at this time. However, the current assumption appears to be indirectly

substantiated by the significant extent to which the quasi-steady blade element hypothesis produces correlation. Thus, rotor performance prediction consists of determining and integrating distributed airfoil section characteristics based on local flow conditions and that unique parameter of CC rotors, the jet momentum coefficient.

The strictly proper parameter for characterizing boundary layer control effects is the coefficient C_{BLC} as defined in the literature. However, the closely related (and much more convenient) parameter, the jet momentum coefficient C_μ , if properly applied, can be used as the basic parameter in characterizing airfoil performance and in defining the boundary layer control level on the rotor. A conversion of C_μ to C_{BLC} is performed within the analysis code where necessary; e.g., to account for slot height effects. The C_μ is simply obtained from the local duct pressure (P_d) and slot height (h/c), assuming isentropic jet expansion (V_j) to the free stream static pressure as follows

$$C_\mu = \dot{m} V_j / (c q)$$

or for incompressible flow

$$C_\mu = 2 P_d h / (c q)$$

It should be noted that, in general, the slot height will be a function of duct pressure due to structural flexibility. For highly flexible slot designs, the external airfoil suction pressure must also be estimated within the performance code to give the net force on the slot nozzle. This slot expansion is actually a desirable design feature in that C_μ , and hence lift, become a stronger function of duct pressure.

Blade duct pressure is based on root pressure level, to which flow losses and centrifugal pressure rise effects as determined from static and whirl tests are added. Centrifugal effects are usually sufficient to offset the duct losses thereby generating a tip pressure somewhat larger than the root level. In fact, there may be certain applications of CC rotary devices for which the rotor can inherently supply all of the pressure rise required for the boundary layer control system. The Coriolis pumping power associated with the duct flow is taken as a shaft power requirement together with the blade-induced and profile power.

Root pressure is either a given function of azimuth, or is obtained from the control valving loss characteristics for a specified control setting. Duct pressure phase lag (root-to-tip pressure change time delay) generally has been found to correspond to sonic velocity.

The pneumatic lag can be of significance at the higher tip speeds, and can be readily modeled analytically. This *blade duct* lag should be distinguished from the additional lag between control valve area change and resulting blade root pressure change. The latter is more of a capacitance effect and can be offset operationally by leading the control input. Once the duct pressure is known at all points on the disc and with angle-of-attack obtained from the inflow theory (to be discussed later) C_l , C_d , C_m can be determined.

3.2 Airfoil Data Base

Numerous two-dimensional blown airfoils have been designed and evaluated by DTNSRDC in the past decade. These tests have generally covered an angle-of-attack range of -20 to +10 degrees which, depending on blowing level, are approximately the angle-of-attack stall limits. Such section performance data is available for airfoils quite similar to those at the root and tip of the RBCCR (References 8 and 9). These two sets of data have been placed in a table lookup routine, with C_l , C_d , C_m as a function of C_μ and angle-of-attack, an example of which is given in Figures 4 and 5. The drag coefficient includes the thrusting effect produced by the jet momentum flow. Performance at intermediate span locations is obtained by linear interpolation between root and tip performance. Thus, an accounting for the influence of geometric factors such as thickness, camber, and trailing edge contour is made. The additional factors of slot height (h/c), Mach number, yaw angle, and Reynolds number must be considered in obtaining the final coefficient values appropriate to the local rotor operating condition.

Over wide ranges of slot height, aerodynamic performance is independent of slot height if the parameter C_{BLC} is used rather than C_μ . Consequently, slot height effects are accounted for through conversion of C_μ to C_{BLC} using potential flow estimates of flow conditions in the vicinity of the slot. Mach number effect algorithms are empirically based on data from a transonic test of a 15 percent blown ellipse (Reference 10). The trends of lift, drag, and moment from this test are applied to all airfoil geometries with appropriate consideration given to relative differences in predicted critical Mach number. Further two-dimensional testing is planned to expand the compressibility effect data base.

At high advance ratio, large excursions in local Reynolds number and yaw angle are experienced that cannot be neglected. Unlike a conventional rotor, significant forces will be obtained in regions of low dynamic pressure because of Coanda blowing. This is seen from the expression $C_\mu \approx 2 P_d h / (c q)$, which indicates how C_μ increases with decreasing dynamic pressure, thus producing less change of lift with q than would be the case with conventional airfoils. Relative influences on lift of Reynolds number and yawed flow were evaluated using a single RBCCR blade as a fixed wing of aspect ratio 8. The effect of yawed flow at a constant chordwise Reynolds number is to delay stall to higher values of C_l (Reference 11). Conversely, at a fixed yaw angle, increasing the Reynolds number results in increased lift at all blowing levels. All of these influences have been incorporated in the aerodynamic tables for both single and dual slot blowing conditions. There is a separate calculation of the skin friction drag due to spanwise flow in the large regions of highly yawed flow.

Effects of simultaneous leading and trailing edge blowing on lift and drag were obtained from the two-dimensional evaluation of the RBCCR tip section profile (Reference 9). This dual blowing generally decreases the lift that otherwise would be obtained with a single slot configuration. Blowing only at the leading edge has been found to have little effect.

3.3 Aerodynamic Environment

Angle-of attack distribution is obtained from the induced flow field calculations. Simple actuator disc momentum theories have generally been considered adequate for conventional helicopter performance analysis; however, the nature of the X-Wing operating environment is such that more sophisticated inflow modeling may be essential.

Of initial interest is the proximity of the wake passage to the plane of rotation. The wake deflection angle is approximately equal to $\tan^{-1} (0.5 C_T / \mu^2)$ indicating a deflection angle of less than 2 degrees at 0.7 advance ratio. For peak efficiency, the thrust-compounded X-Wing is expected to operate at a nose-up positive shaft angle ranging from +2 to +7 degrees. This would then place the plane of rotation within a few degrees of the wake trajectory in contrast to the condition for conventional helicopters (Figure 6). The inplane blade-vortex intersections that can occur are considered next. Figure 7 illustrates, from simple geometric considerations, tip vortex path and blade intersections at 0.7 advance ratio. Vortex crossings particularly impact the fourth quadrant from 270 to 360 degrees. (Reference 12 contains a detailed discussion of these geometric relationships.) The blade is, in effect, operating within its own wake for a quarter of a revolution. The trajectory of the root vortex which impacts along the longitudinal axis is not shown. This root wake can be quite significant because of the large loading generated in the reverse flow region when dual blowing is employed.

Another perspective on the rotor operating environment is obtained from an examination of the disc loading distribution. Figure 8 presents the analytically predicted blade thrust (lift) distribution for a typical high speed, trimmed flight condition. This prediction used vortex inflow theory (to be discussed later). The resulting integrated forces correlated with the corresponding wind tunnel data point. A number of relevant characteristics of CC rotors can be seen here. First, there is a rather large region of negative lift on the advancing side. This results from the shaft angle and blade collective angle producing a negative incidence on the advancing side. With the blowing coefficient being low due to high dynamic pressure, there results a negative lift coefficient. This negative lift appears to be a requirement for roll trim, at least for the current rotor design. The highest positive lift occurs fore and aft. Of course, the azimuthal load distribution is controllable by the pressure valving system. For example, the fore/aft load can be further enhanced if a 2p pressure control waveform

is applied. Of relevance to the inflow modeling is the strength of the tip vortex generated in the third quadrant, because it will impact in the fourth quadrant.

The reverse flow region with its dual blowing is indicated as producing heavy load inboard, which would generate a strong root vortex also passing through the fourth quadrant. There are controlling pressure waveforms that would substantially increase this load.

In summary, the rotor loading is highly nonuniform with regions of negative thrust. Such a distribution would certainly raise doubts about the applicability of uniform downwash inflow methods, especially because the negative thrust region would be given the same inflow as the heavily loaded regions. In addition, numerous close blade/vortex passages will occur due to the shaft angle and advance ratio. The strength of the vortices involved depends on the azimuthal load-control pressure waveform, while the vortex passage proximity is shaft angle dependent. It would seem that the inflow mathematical representation must consider all of these factors; however, it remained to be seen just how sensitive the predicted rotor performance was to the degree of inflow sophistication.

3.4 Inflow Representation

The rotor inflow field definition at high advance ratios proved to be the most difficult portion of the analytical development and correlation effort. Progressively more rigorous methods were employed, eventually culminating with the most sophisticated techniques available.

Uniform inflow with the Glauert longitudinal distribution had initially been used for CC rotor design and performance analysis. Its simplicity and low computational cost were decided advantages. When the first high speed rotor wind tunnel data became available, the roll moment and thrust did not correlate with predictions. This tended to confirm doubts about the adequacy of the uniform momentum approach. Efforts were then undertaken to develop or acquire more appropriate inflow models.

As an interim measure, the uniform inflow method was modified to a "distributed momentum" concept. This approach was intended to provide a first approximation to the inflow produced by highly nonuniform disc loading. The technique consists of locally multiplying the uniform inflow value by the local relative thrust loading, as based on either blade area or disc area. This approach produces upwash in regions of negative lift while placing the highest downwash velocity at points of highest load (Figure 9), thus approximating the physics of the rotor more realistically. The resulting average of the downwash is unaffected, which means that the blades still see a time averaged inflow. Load distribution is based on local disc area loading for hover and low speeds and is analogous to the familiar annular momentum theory in hover. For the higher advance ratios, as the rotor approaches a fixed wing mode of operation, a loading based on thrust per unit blade area was considered. The changes produced in predicted performance when these methods were applied will be discussed later.

The next improvement in inflow validity was obtained through the application of vortex theory. The mathematical derivations found in Reference 13 were used to develop what this reference calls a "quasi-linear" inflow solution (in actuality, a potential disc theory). This particular approach, one of several in Reference 13, assumes a skewed cylindrical wake of continuous vorticity and therefore is unable to account for finite blade effects, such as vortex passages. Its primary advantage was low computational cost for routine performance calculations.

The final computational model employed the full vortex lifting line development of Reference 14. This free wake solution most closely represents the physical phenomena by calculating the instantaneous induced velocity (i.e., the induced velocity as experienced by the blade). It also tracks the vortex in space and thereby contains the inherent capability to model the local effects of a vortex encounter. For example, the findings of Ham¹⁵ concerning the maximum lift increment produced by a close vortex/blade passage could be incorporated. Both tip and root vortices are represented (Figure 10). High computational cost had previously limited

the application of full vortex theory to those situations where it is essential, such as acoustic investigations. However, as will be demonstrated, vortex theory is also essential for general performance analysis of high advance ratio CC rotors. Computer costs have been reduced to an acceptable level by using an "influence coefficient" matrix that can be stored and reused later for similar flight conditions. This matrix is the end product of the vortex calculations with the actual inflow obtained by multiplication with the circulation distribution. The induced velocity at any point is described by

$$V_{ij} = \sum \sigma_{ijk1} \Gamma_{k1}$$

where V_{ij} is the induced velocity at the radial station i for the blade at azimuth j . The Γ_{k1} is the bound circulation at the radial station k for the blade at azimuth position 1 . The σ_{ijk1} is the influence coefficient matrix. Summation is over all the radial and azimuthal points of the blades. A significant cost reduction is also possible by utilizing the undistorted wake (fixed helical) option in the computer model. It has been found that the helical wake generally gives adequate performance correlation relative to the free wake representation. However, there may be special circumstances in which the free wake accuracy is needed so that this option has been retained.

Table 2 summarizes the major features of the inflow methodologies discussed above. A part of the correlation task was to evaluate these inflow representations and to identify any circumstances in which the simpler methods would be acceptable.

4. PERFORMANCE CORRELATION

Concisely stated, the correlation objective was to develop the capability to analytically duplicate wind tunnel results over the full range of available data. Emphasis was placed on high advance ratio operation, since other CC projects had established correlation at low speed primarily through identification of slot height and Mach number effects (Reference 7). Shaft angle ranges covered included those that should produce wake passages under, over, and through the rotor plane (0 to 5 degrees shaft inclination). A full range of azimuthal load distributions, or pressure waveforms, were examined for each shaft angle. Accurate prediction of roll moment generated for a given control setting was of particular concern because, for CC rotors, required peak pressure is related to roll trim requirements. Also, thrust produced for a given pressure and mass flow must be known accurately since compressor power can be as much as 80 percent of the total rotor power required in conversion flight. Blade loading and dynamic response was not a part of this correlation effort although the mathematical model has been applied recently to the results of the 25-foot rotor test.

4.1 Correlation Procedure

Wind tunnel data used in the correlation consisted of balance readings, total mass flow, and oscillograph tracings of the internal duct pressure. There are two ways this data can be used in correlation. First, the trimmed data points can be plotted along with analytically trimmed points in, for example, a comparison plot of thrust versus compressor power. However, in general, the analytical point will have a different control setting in terms of peak pressure, mass flow, or cyclic waveform. Thus, such plots alone do not directly reveal all the details of just how closely the theory is matching experiment. The second approach (the authors preferred method) is to take an individual data point and duplicate within the analysis the same control settings and wind tunnel conditions. In this way the analytically predicted moments and forces can be compared directly to the balance readings in a table format thereby providing more insight into any theory/experiment differences. This approach is advantageous when there is an initial lack of correlation and there are as many operating parameters influencing performance as there are on the RBCCR. This procedure is somewhat tedious, in that it requires that the azimuthal pressure wave traces be accurately digitized and placed in a table lookup routine for access by the analysis. However, there is a distinct advantage in that this procedure removes any concern over whether the experimental pressure harmonic content is being correctly modeled analytically. Accuracy of the pressure data is of the utmost importance, because even a 10 percent error in the pressure

reading, due to temperature effects for example, can make a 15 to 20 percent difference in the predicted forces. If dual blowing is used, leading edge duct pressure is input separately since the two ducts do not always have the same pressure level.

The initial step in the RBCCR correlation was to establish a representation for the spanwise duct pressure distribution based upon the known root pressure. One blade was equipped with three spanwise pressure transducers. Static flow test data was used to empirically establish flow loss factors with whirl stand data used to determine the centrifugal pumping effects. Pressure at any point is calculated as the sum of duct loss and centrifugal pressure rise effects. Pneumatic phase lag between root and tip of the RBCCR at normal test rotational rate is about 9 degrees. However, this lag is not normally modeled since it is small and there is thought to be an uncertainty in the phase angles of about 6 degrees due to instrumentation system phase shifts. The primary effect of any lag would be to interchange predicted roll and pitch moments slightly. Blade dynamic response lags for this 2.3p to 2.7p flatwise frequency rotor are considered negligible.

Next in importance is establishing correlation between mass flow and blade root pressure. At each span position, slot height measurements from all eight of the RBCCR slots were averaged to define a mean blade slot height distribution for the rotor geometry description input. This distribution was used to check calculated versus measured mass flow for a number of rotating data points. The analysis was found to overpredict the flow rate by about 5 percent; consequently, the assumed slot height was reduced by 5 percent (this may be a discharge coefficient effect or a height measurement bias). Thereafter, the mass flows were nearly always well within 5 percent agreement. Without such a pressure-mass flow match, a correlation of performance cannot be valid. At this point, the rotor pneumatic characteristics and control inputs were represented with sufficient accuracy to enable the force, moment, and power correlation to proceed.

4.2 Correlation Results

Table 3 presents the results of one of the earliest data points analyzed. Here, both trailing and leading edge pressure waves from the test have been fed into the analysis along with a full specification of rotor and tunnel conditions. Note that the mass flow is within 3 percent of the measured value. The benefits of using increasingly sophisticated inflow theories are clearly evident. Uniform inflow predicts a roll moment which is in substantial disagreement (thrust vector offset is 20 percent of radius from shaft center) with the tunnel results. With modification to a distributed momentum inflow there is improvement in both roll and pitch. The linear (or quasi-linear as it is referred to in Reference 13) vortex development makes a further gain in roll correlation but not in thrust. (Recall that all but the full vortex models give time averaged induced velocities whose mean value corresponds to the results of actuator disc theory.) Only the full vortex method, in this case a fixed helical wake calculation, correlated with all major parameters. For this data point, the thrust level without blowing was minus 27 pounds indicating a thrust due to blowing of 91 pounds which gives a blowing thrust correlation within 5 percent. Rotor drag is not presented for comparison to prediction because of the uncertainty in the drag data resulting from the low drag force levels and tares. The torque, which constitutes about 28 percent of the total power in this case, did not correlate as well when vortex theory was used. This may be a result of the profile drag coefficient data base not covering the extreme incidence angles that vortex theory predicts for the fourth quadrant.

As expected, the velocity distribution predicted by the vortex method is substantially different from that obtained using the momentum approach. Figure 11 compares the two inflows for the 80 percent span station at zero shaft angle. Both indicate regions of upwash which strongly influence the roll moment predictions. The large excursions in downwash can be identified with the root and tip vortex passages. According to the vortex model, peak inflow results largely from the shed wake in the reverse flow circle. For this reason the downwash in the fourth quadrant is quite different if dual blowing is not applied. There is no data available to directly verify the accuracy of the inflow predictions. The vortex computer code of Reference 14 was originally correlated at low advance ratio using flow field data. To do the same at high advance ratio for CC rotors would require acquisition of data through means of a laser velocimeter survey – a substantial undertaking.

The approach taken by DTNSRDC has been to infer validity of the inflow model of Reference 14 by the degree with which it gives rotor performance correlation over widely different operating conditions. To an extent, wind tunnel data has been acquired for unusual configurations solely for the purpose of correlation checks. For example, could the differences between dual and single slot blowing on the retreating side be accounted for? The predicted downwash in the fourth quadrant for these two cases would be quite different. Table 4 presents the results of such an experiment. Data was acquired by first trimming the rotor with dual blowing to a thrust level of 70 pounds. Then while keeping the controls fixed, the rotor was stopped to tape over the leading edge slots to prevent any possible blowing. Data was then recorded for this single slot configuration. These two data points were separately input to the analysis program. Table 4 compares the force deltas which represent the effect of applying reverse blowing experimentally versus analytically. The agreement obtained can be considered within the range of experimental uncertainty. Note the beneficial effects of dual blowing which substantiate the original RBCCR concepts. It is recognized that using this approach to establish confidence in the inflow model assumes that no other inadequacy in the analysis is providing compensatory trends. For example, the blade element approach assumes that the reverse flow region is well-behaved with no unpredictable flow separation or other unaccounted for phenomena.

Earlier versions of the analysis, without the vortex based inflow, could not accurately account for shaft angle trends or load distribution effects. Therefore, the final evaluation of the vortex theory at advance ratio 0.7 was to compare with data at the shaft angles of 0.0, 2.5, and 5.0 degrees. For each shaft angle, three widely different azimuthal control input distributions (Figure 12): 1p, +2p (longitudinal loading), and -2p (lateral loading) were examined. All experimental trends were found to be analytically predictable.

In addition to these points, all of which were at $C_T/\sigma = 0.09$, a data point at $C_T/\sigma = 0.11$ was selected as representing the highest thrust needed by a flight demonstration vehicle. Table 5 presents this last point. Except for the shaft torque, vortex theory provides quite satisfactory agreement. For most of the cases examined, pitching moment does not correlate as well as it did here (for example, see Table 6). The similarity between the pitching moments predicted by momentum and vortex methods (Table 6) is typical. The common factor in the degree of pitch correlation seems to be the azimuthal loading with a lateral loading producing the largest discrepancy.

Low advance ratio conditions from 0.2 to 0.5 were also examined. Table 7 presents a typical case at an advance ratio of 0.30 and zero shaft angle. Once again only the vortex inflow gives the correct rolling moment, although the usual uniform momentum inflow does predict the other moments and forces. The distributed momentum approach would therefore appear to be a reasonable compromise between accuracy and cost at the lower advance ratios although a final conclusion in this regard would require additional wind tunnel data at shaft angles of interest for low speed operation. This data is not available for the RBCCR.

Figure 13 summarizes the correlation results using fixed helical wake vortex theory. Each symbol represents a data point which was analytically duplicated. Thus, the dominant power term, the compressor power, is in agreement. Roll and thrust are considered to be in satisfactory agreement. Shaft power (torque), as seen earlier, is overpredicted in a consistent manner. This is believed to be due in part to a lack of valid drag representation at the extreme blade element angle-of-attacks encountered ($\alpha < -20$ degrees) and also possibly to excessive induced drag produced theoretically by unrealistically high vortex core velocities. It is planned to analytically explore the sensitivity of these factors further.

Pitch does not correlate as well as desired. An interesting observation, not shown in the data presented here, is that using the Glauert factor with momentum based inflow gives essentially the same relative pitch correlation. With the strongest vortex/blade intersections occurring in the rear of the disc, the factors causing the discrepancy in pitch may be the same as those for the torque mentioned above.

4.3 General Performance Prediction Procedures

The procedure for correlation required that the rotor control settings be specified as an input to the performance analysis code. The more general use of this routine is to find pneumatic control settings and power levels that will produce trimmed flight.

Flight control variables are shaft angle, collective angle, mean duct pressure level, and the percent of cyclic pressure modulation in the roll and pitch axis. The equation for blade root pressure is

$$P(\psi) = P_{\text{col}} [1 - A \sin(\psi) + B \cos(\psi) + C \sin(2\psi) + D \cos(2\psi)]$$

where P_{col} is the mean, or "collective," root pressure relative to ambient pressure.

The 2p phasing coefficients C and D are for optional use to fine tune performance for either blade load control or peak thrust, as will be discussed later. The azimuth range for dual blowing is also specified. Primary thrust control is through P_{col} . Pitch moment is controlled by the cosine coefficient B while roll control has two options: cyclic pressure (A) or collective pitch angle θ_c . It has been found that analytical convergence to trimmed flight is faster at the higher advance ratios if collective angle is used as primary roll control.

An initial performance solution is obtained using estimated control settings with distributed momentum inflow, which is followed by an entry into the vortex inflow subroutines. The principal output from these subroutines is the influence coefficient matrix which, when multiplied by the disc circulation distribution, gives the inflow. This matrix is usually 200×200 (10 span stations and 20 azimuths) and may be stored for later use if the same advance ratio and equivalent wake skew angle conditions are to be rerun later. There is no further entry into the vortex subprograms. The input control settings are now rerun using the vortex inflow.

In general, the rotor will initially be out of trim. Each primary control setting is then incremented separately to obtain a 3×3 matrix of control sensitivities and interactions. This matrix is solved for settings that should produce trim at the desired thrust. If trim does not result, this procedure is repeated. In a typical computer run, most of the computing time is actually not in the vortex code but is in extracting the aerodynamic coefficients from the two-dimensional performance algorithms. Typical execution time on a CDC 6600 is 250 seconds.

5. RELATED EXPERIMENTAL INVESTIGATIONS

5.1 Flow Visualization With Tufted Blades

Analytically, it is assumed that the region of dual blowing and reverse flow behave in a manner consistent with the quasi-steady strip theory. Except for local vortex disturbances, the analysis predicts no regions of separated flow at operational flight conditions. As a qualitative check of the rotor flow conditions a digitally controlled photographic strobe system was designed and built. All four blades were tufted, each with a different chordwise tuft position. The digital system permitted direct specification of the azimuth to be photographed with real time visual observation also possible. Figure 14 shows a blade with both slots blowing that has just entered the expected reverse flow region. The advance ratio is 0.7 with a positive shaft angle of 2.5 degrees. The inboard tufts have flipped over and clearly indicate a stable region of reverse flow. Note the tuft near the mid-span which is standing straight up (its shadow can be seen) as the flow reverses direction. (Centrifugal force influences must be considered when interpreting these photographs of course.)

Figure 15 is a similar photograph, but with the blade in the fourth quadrant. Here the tufts are slightly disturbed compared to those in the forward quadrant. Vortex theory predicts the beginning of root and tip vortex influence at this position. Detailed inspections of blade positions between 305 and 332 degrees (not pictured here because of reproduction difficulties) reveal that, at the points of expected tip vortex intersections, the tufts on approximately 10 percent of the span lie in a spanwise direction, out of line with adjacent tufts. This suggests that the flow is locally separated, with tuft position dominated by centrifugal force or spanwise flow.

No major regions of separated flow were observed on the rotor. Tuft positions were quite steady, apparently as a result of the Coanda sheet entrainment effects. It would be interesting to repeat this investigation at the limits of rotor thrust - a limit that has not as yet been reached even at $C_T/\sigma = 0.24$ at 0.7 advance ratio. In summary, nothing was observed experimentally that invalidates the fundamental assumptions in the

analytical developments. The extremely clean airfoil aerodynamics is fortuitous for analytical modeling and once again illustrates the powerful effect of the Coanda boundary layer control on "calming" an otherwise severe flow environment.

5.2 Blade Profile Pressures

In the May 1979 test of the 25-foot X-Wing rotor (similar to the RBCCR), one of the blades was instrumented at the 72 percent span position with 16 surface pressure transducers in addition to internal duct pressure and slot height transducers (Figure 16). The purpose was to provide a direct look at the unsteady three-dimensional aerodynamics of blown rotors. Five of the transducers did not function properly and the electrical signals were contaminated with noise which has not been completely filtered out yet. One of the ways this data is being used is to obtain an estimate of the lift coefficient and angle-of-attack for eventual comparison to that predicted by the rotor program. This lift coefficient and flow inclination determination is a trial and error procedure of varying the lift and angle-of-attack inputs to a potential flow airfoil analysis until the best match to the actual pressure is obtained. An example obtained at advance ratio 0.4 is shown in Figure 17 where the angle-of-attack was deduced as being -10 degrees with a positive lift coefficient of 0.81. (This is representative of CC rotor operation.) Achieving such a degree of pressure correlation suggests a minimal influence of unsteady flow as might arise from time varying blowing, angle of attack or velocity.

5.3 Higher Harmonic Control

For the most recent RBCCR model wind tunnel entry a Fast Fourier Transform computing spectrum analyzer was used to examine the unsteady data channels. Of particular interest was the effect of the inherent and irreducible 8 cycles per revolution (8p) pressure wave component produced by certain design aspects of the eight segment valving configuration being used. The blade flatwise bending moment was analyzed for indications of response to this 8p pressure modulation which is 96 hertz at model scale. The results are presented in Figure 18. The moment shows a definite 8p, 9p, and 10p content (the plot is off scale for the 2p and 3p moments). This characteristic is tentatively interpreted as a response to the 8p pressure with the 9p and 10p a result of the nonlinearity of lift due to pressure and to the 1p dynamic pressure variation interacting to give other frequency components (harmonic distortion) of blade lift and moment. Also the blade second natural flatwise frequency is at 10.8p, consequently the 9p and 10p forcing functions would be expected to receive amplification compared to 8p. It should be noted that, since there was no way to eliminate or change the 8p input, there was no way to prove that these responses were due to the pressure. No blade dynamic analysis has been performed to determine the degree of correlation of this higher harmonic response with quasi-steady theory. However, a simple check was made, as described below, to see if the 9p, 10p frequency components could be expected to result from an 8p control input. A simple model for the aerodynamic loading can be obtained as follows. Let the bending moment M be represented by the lift L acting at radius r. Also let the CC airfoil lifting characteristic be represented by the approximation $C_L \approx 14\sqrt{C_\mu}$

$$\text{then, } M = Lr = q C_L r = q r 14\sqrt{C_\mu}$$

$$C_\mu = \frac{2 P_d h/c}{q}$$

$$\text{with } P_d = A - B \sin \psi + C \sin 8\psi$$

$$q = (V_T r + V_\infty \sin \psi)^2 \rho$$

$$\text{giving, } M(\psi) = 14r \sqrt{(h/c) (A - B \sin \psi + C \sin 8\psi) (V_T r + V_\infty \sin \psi)^2 \rho}.$$

A frequency analysis of this equation reveals, as was observed experimentally, substantial 7p, 9p, and 10p harmonics in addition to the fundamental 8p. It thus appears that the CC rotor is capable of achieving high frequency pneumatic response.

To establish the feasibility of higher harmonic control, a decision was made to demonstrate the open loop reduction of a selected moment component by pneumatic control. With 2p being the dominant flatwise moment when using the standard control pressure wave (1p) it was targeted for the reduction attempt. A frequency spectrum analyzer displaying blade moment levels in near-real time was placed in view of the rotor operator with instructions to find a pressure wave that would reduce the 2p moment while maintaining the same thrust and trim. (The valving arrangement was such that each 45 degrees of azimuth had an individual pressure valve.) This attempt was completely successful (Figure 19) with the 2p subsequently eliminated entirely. Success with other bending moment components such as 3p may not be so readily achieved unless a more versatile (additional segments) valving system and automatic control loop is used.

The results of a more systematic experimental investigation of the influence of 2p pressure content is presented in Figure 20. Here three levels of 2p were input with the rotor retrimmed at the same thrust for each data point. The 2p control influences both bending moment and lift system efficiency in that the power required for a given thrust depends on the 2p control level and phasing. Efficiency is highest for a positive 2p input (pressure peaking fore and aft on the disc) whereas bending moment is lowest for the negative 2p phasing (lateral pressure peaks). Note also that the 3p moment which is the primary source of 4p shaft moments, is simultaneously reduced with the 2p. A similar result was also obtained on the 25-foot rotor in the Ames wind tunnel. An analysis similar to that preceding for the 8p pressure reveals that the moment response to a 2p input has 1p and 3p components, with the phase of the 3p component offsetting that inherent in the rotor.

These findings have confirmed the potential of readily achieving higher harmonic control in CC rotors with fixed system (nondynamic) controls. They also illustrate the performance tradeoffs and the frequency input/output factors required in design of operational control systems.

5.4 Flatwise Frequency Placement

In conjunction with the 2p pressure wave experiment an investigation of the influence of the blade first flapping frequency placement was performed. The RBCCR, while not dynamically scaled, does have first and second flatwise blade natural frequencies within the expected full scale design range. Of interest is the relative magnitudes of the 2p and 3p blade moments as the rotor rotation rate is varied to move the ratio of flatwise to rotational frequency through the range of 2.0p to 3.0p. The results, shown in Figure 21, have been adjusted to correspond to a constant disc loading and are for a 1p pressure wave. Trends are as expected, with 3p increasing as 2p diminishes with increasing frequency placement. With 2p moment so readily controlled by the valving system a desirable operating point might be around 2.3p.

6. SUMMARY AND CONCLUDING COMMENTS

The application of circulation control technology to rotors adds several new aerodynamic parameters to the design process while significantly expanding the possible operating regimes for rotorcraft. The development and validation of analytical procedures to supplement the experimental evaluations is imperative in order to fully exploit advanced concepts.

The extensive subscale rotor data base generated at DTNSRDC has been used in evolving correlated analytical methods for application to high advance ratio flight. A major factor in the success achieved so far has been the employment of a vortex wake computational model. At all advance ratios examined (0.3 to 0.7), only the application of a vortex based inflow resulted in the correct prediction of both roll moment and thrust for the hingeless RBCCR rotor.

Of profound significance is the finding that with the proper inflow model, the extensive CC airfoil data base now available can be used directly in a quasi-steady blade element approach to rotor performance prediction even in highly adverse aerodynamic environments. The concept of "lift independent of flow direction," that is, reverse or dual blowing on the retreating side, has been substantiated by flow visualization studies. The

agreement between analysis and experiment with regard to the influence of dual blowing also indicates that the reverse flow region can be a productive area of the disc.

The potential of higher harmonic control has been demonstrated by the virtual elimination of the 2p flatwise moment. Nonlinearities between duct pressure and lift in the rotary environment can produce secondary harmonics. Fortuitously, this results in the ability to simultaneously reduce both 2p and 3p moment with a simple 2p pressure input.

Future undertakings in the areas of correlation should include operational scale tip speeds and duct pressures. The potentially significant contribution of a faired hub to the total lifting capability should also be addressed. Higher harmonic control response and phasing requires systematic exploration both by experiment and analytical means with primary emphasis on the experimental approach in view of uncertainties in unsteady aerodynamic and pneumodynamic modeling.

With the advent of a correlated analytical procedure, design optimization studies of the X-Wing and other rotor configurations can be undertaken with renewed confidence. This effort should include integration of new airfoil contours that are becoming available from comparable developments in CC airfoil theory.

7. ACKNOWLEDGMENTS

The author wishes to acknowledge the contributions of his colleagues at DTNSRDC. Support for this research was provided by the Naval Air Systems Command and the Defense Advanced Research Projects Agency.

8. REFERENCES

1. I. C. Cheeseman and A. R. Seed, The Application of Circulation Control by Blowing to Helicopter Rotors. Journal of the Royal Aeronautical Society, Vol. 71, No. 848, July 1966.
2. R. M. Williams and E. O. Rogers, Design Considerations of Circulation Control Rotors. Paper 603, 28th National Forum of the American Helicopter Society, Washington, D.C., May 1972.
3. J. B. Wilkerson, et al., The Application of Circulation Control Aerodynamics to A Helicopter Rotor Model. Paper 28, 29th National Forum of the American Helicopter Society, Washington, D.C., May 1973.
4. R. M. Williams, Application of Circulation Control Rotor Technology to A Stopped Rotor Aircraft Design. First European Rotorcraft and Powered Lift Aircraft Forum at Southampton, England, September 1975.
5. K. R. Reader, D. G. Kirkpatrick and R. M. Williams, Status Report On Advanced Development Program Utilizing Circulation Control Rotor Technology. Vertica Vol. 3, No. 11979, Also Fourth European Rotorcraft and Powered Lift Aircraft Forum, Stresa, Italy, September 1978.
6. A. J. Potthast, X-Wing Stability and Control Development and Wind Tunnel Demonstration Tests - Helicopter, Conversion and Fixed Wing Flight. Preprint 80-27, 36th Annual Forum of the American Helicopter Society, Washington, D.C., May 1980.
7. J. B. Wilkerson and D. W. Linck, A Model Rotor Performance Validation for the CCR Technology Demonstrator. Preprint 902, 31st Annual National Forum of the American Helicopter Society, Washington, D.C., May 1975.
8. R. M. Williams and H. J. Howe, Two-Dimensional Subsonic Wind Tunnel Tests On A 20-Percent Thick, 5-Percent Cambered Circulation Control Airfoil. NSRDC Technical Note AL-176 (AD 877-764), August 1970.

9. J. Ottensoser, Two-Dimensional Subsonic Evaluation of A 15-Percent Thick Circulation Control Airfoil with Slots At Leading and Trailing Edges. NSRDC Report 4456, July 1974.
10. R. J. Englar, Two-Dimensional Transonic Wind Tunnel Tests of Three 15-Percent-Thick Circulation Control Airfoils, NSRDC Technical Note AL-182 (AD 882-075), December 1970.
11. R. M. Williams, R. T. Leitner and E. O. Rogers, X-Wing: A New Concept in Rotary Wing VTOL. Presented at the American Helicopter Society Symposium on Rotor Technology, August 1976.
12. L. R. Lucassen, Ranges and Critical Values of Advance Ratio for Blade/Vortex Intersection Patterns of A Helicopter Rotor. Proceedings of Fifth European Rotorcraft and Powered Lift Aircraft Forum, Amsterdam, September 1979.
13. V. E. Baskin, et al., Theory of the Lifting Airscrew. Moscow, 1973 (NASA Technical Translation TTF-823, February 1976).
14. S. G. Sadler, Development and Application of A Method for Predicting Rotor Free Wake Positions and Resulting Rotor Blade Air Loads. NASA CR-1911, December 1971.
15. N. D. Ham, Some Conclusions from An Investigation of Blade-Vortex Interaction. Journal of the American Helicopter Society, Vol. 20, No. 4, October 1976.

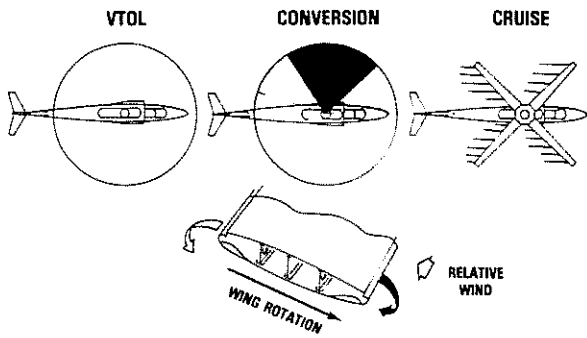


Figure 1 – X-Wing Flight Concept

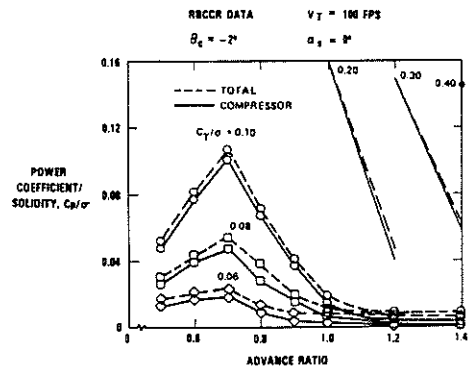


Figure 3 – Power Trends at High Advance Ratio (Experimental Results)

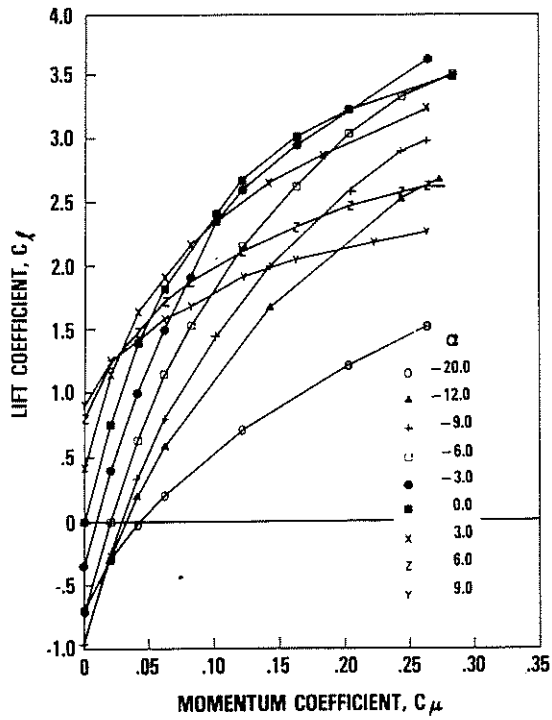


Figure 4 – Lift Coefficient Data for Blade Tip Airfoil Contour

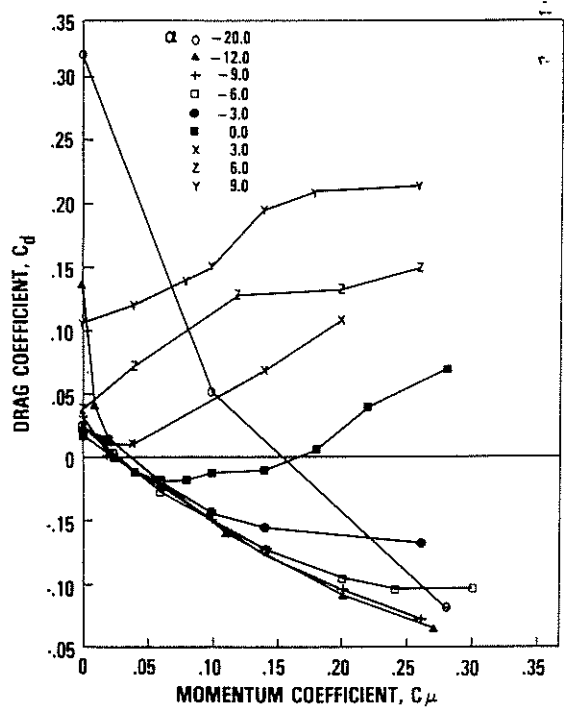
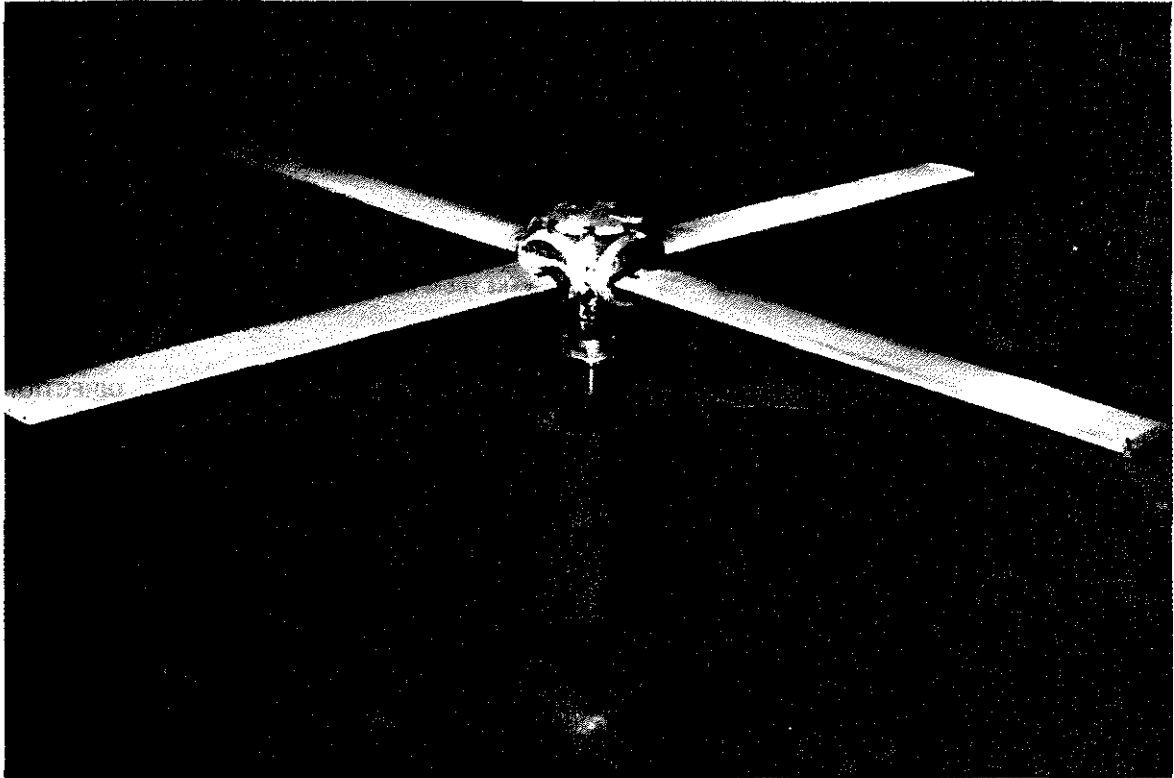


Figure 5 – Drag Coefficient Corresponding to Figure 4



RBCCR MODEL DETAILS

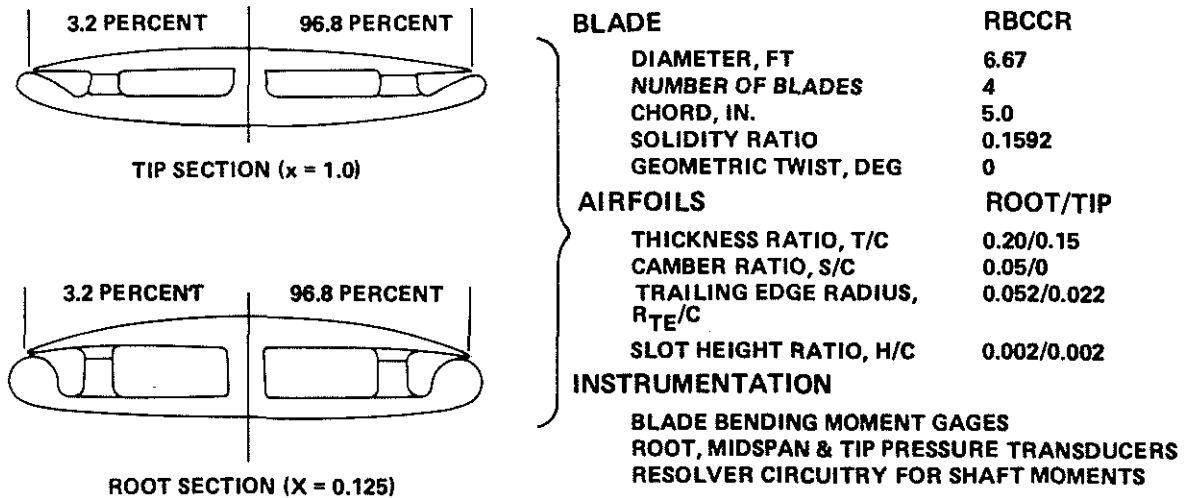


Figure 2 – Description of Wind Tunnel Model (Reverse Blowing Circulation Control Rotor) Used in High Advance Ratio Investigation

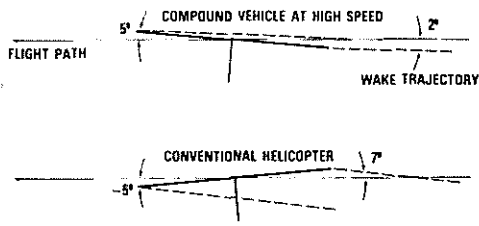


Figure 6 – Wake Skew Angles

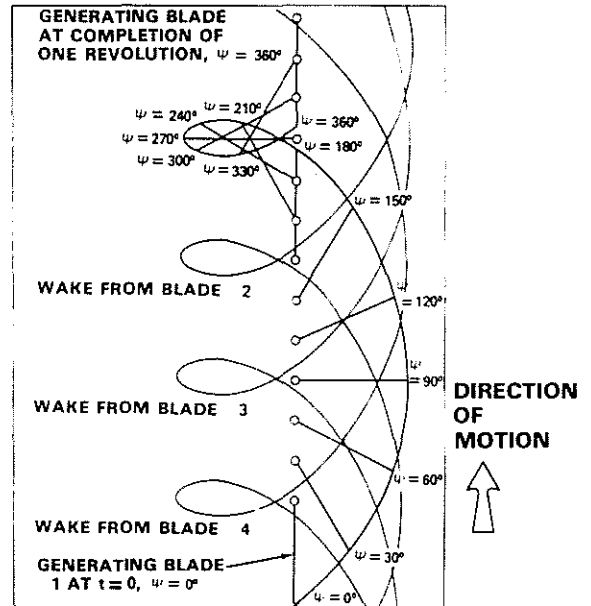


Figure 7 – Tip Vortex Intersections at 0.70 Advance-Ratio

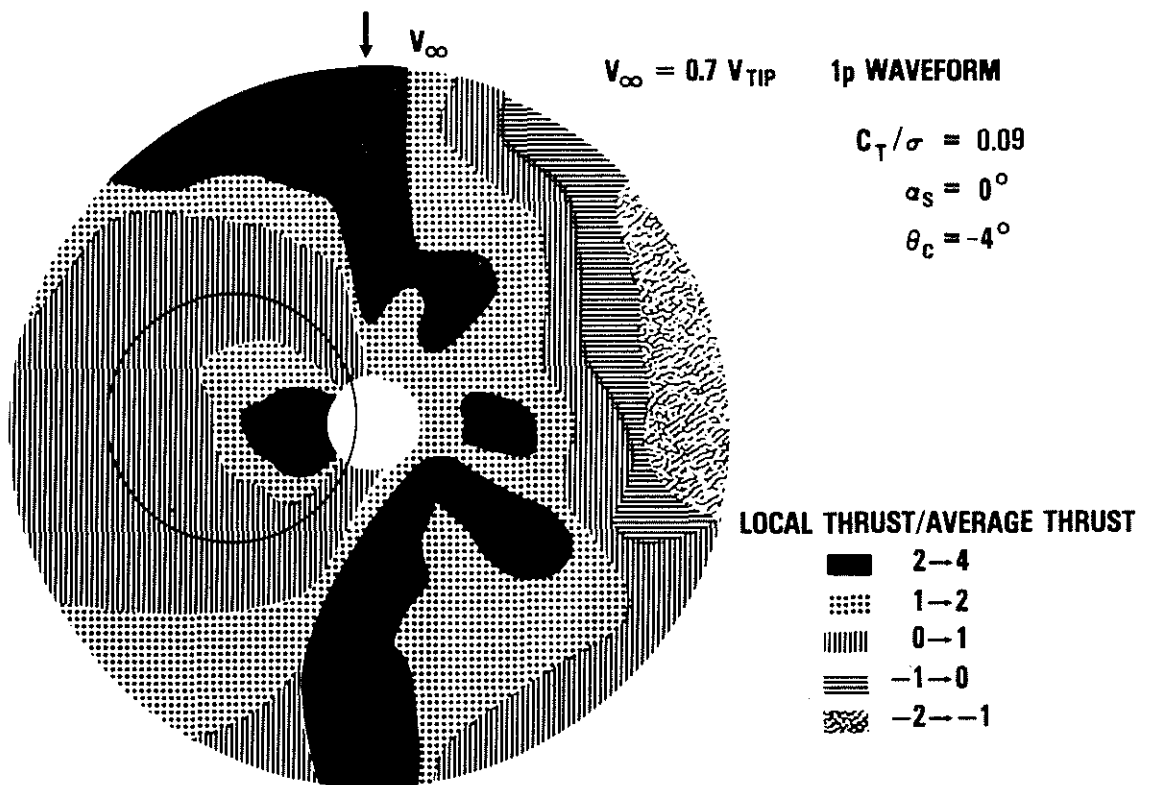


Figure 8 – Predicted Blade Load Distribution in Trimmed Flight (Typical)

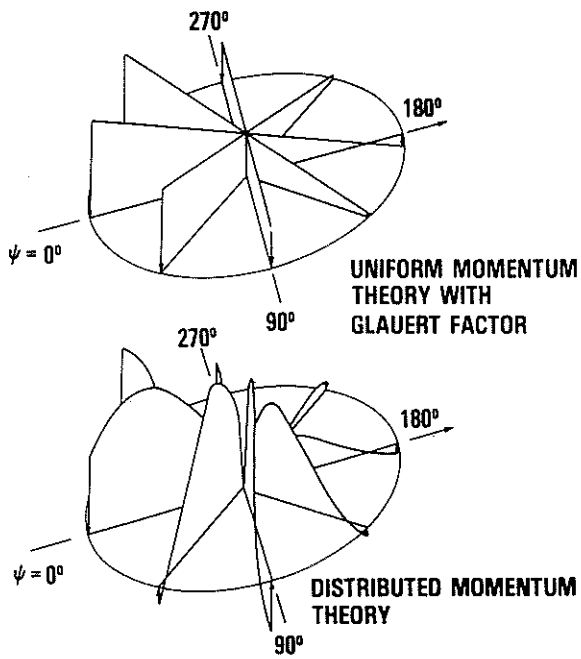


Figure 9 – Inflow Velocity Distribution Produced by the Momentum Methods (Typical, $\mu = 0.7$)

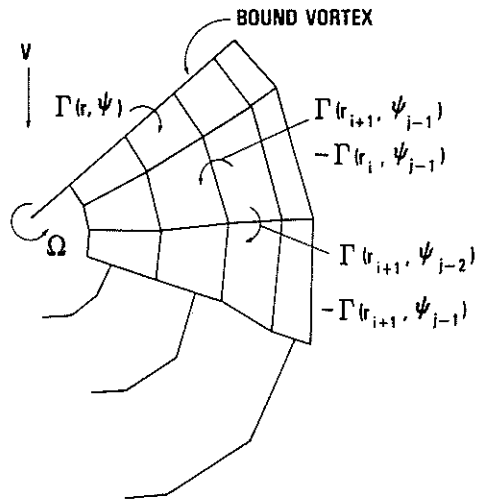


Figure 10 – Vortex Wake Model with Combination of “Full Mesh” Wake of Shed and Trailing Vortices and “Modified” Wake of Trailing Vortices Only (from Reference 14)

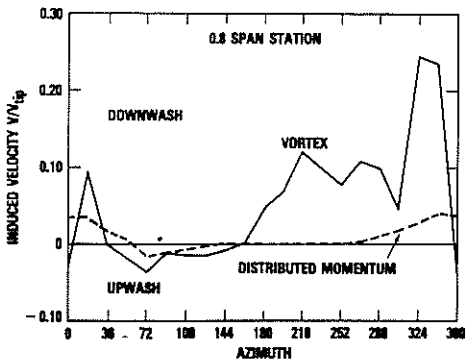


Figure 11 – Inflow Prediction Comparison at Advance Ratio 0.7

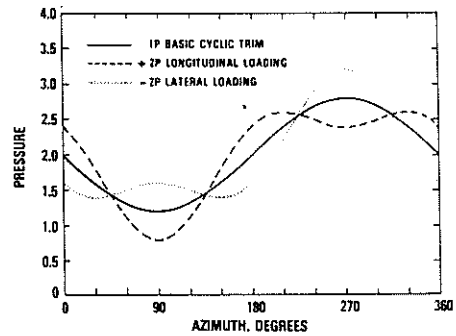


Figure 12 – Basic Pneumatic Control Waveforms

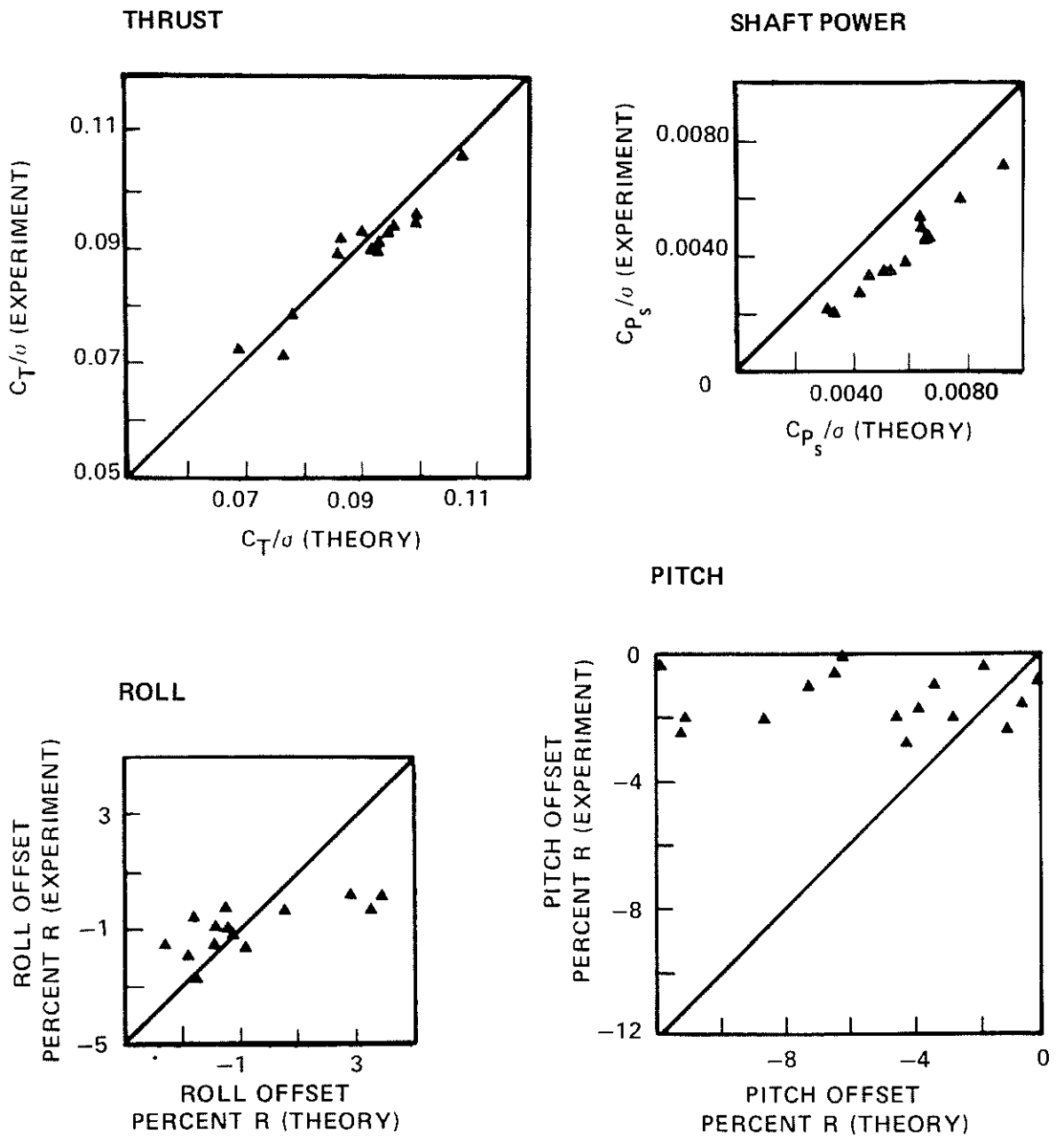


Figure 13 – Correlation Status Summary Over Advance Ratio Range 0.2 to 0.7

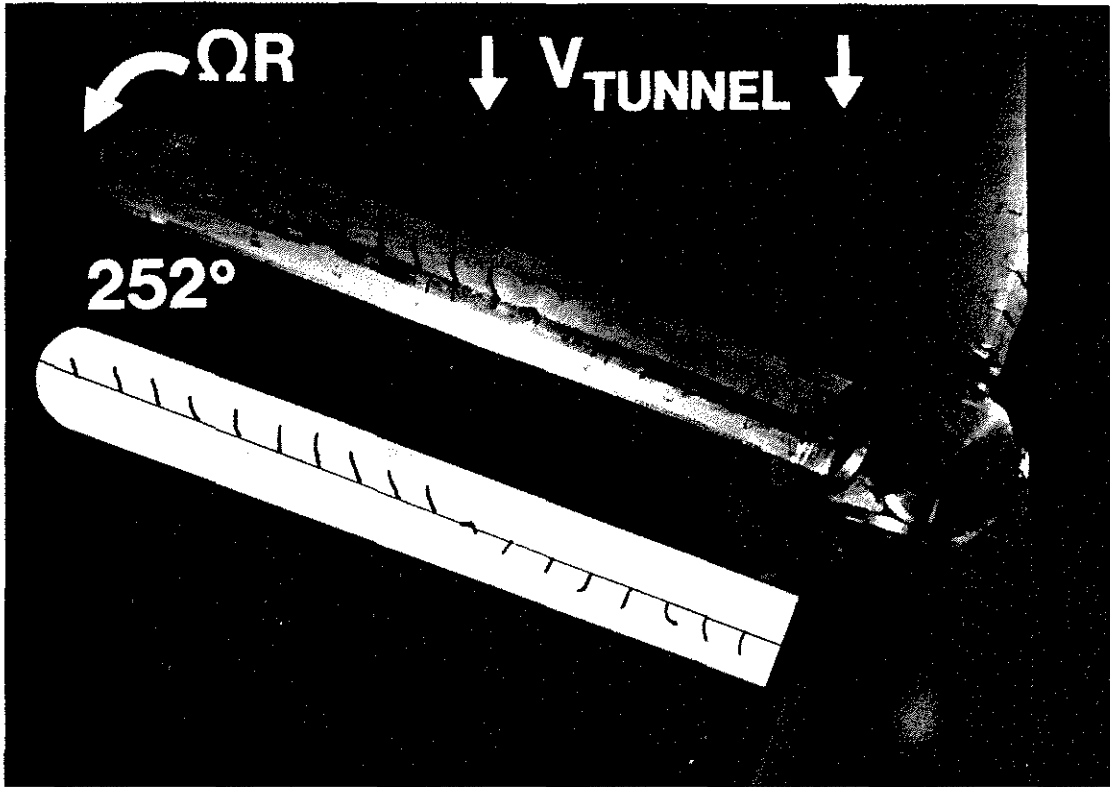


Figure 14 – Retreating Side Photograph of Tufted Blades at Advance Ratio 0.70 with $C_T/\sigma = 0.085$, $\alpha_s = +2.5$, $\theta_c = -4$ Degrees

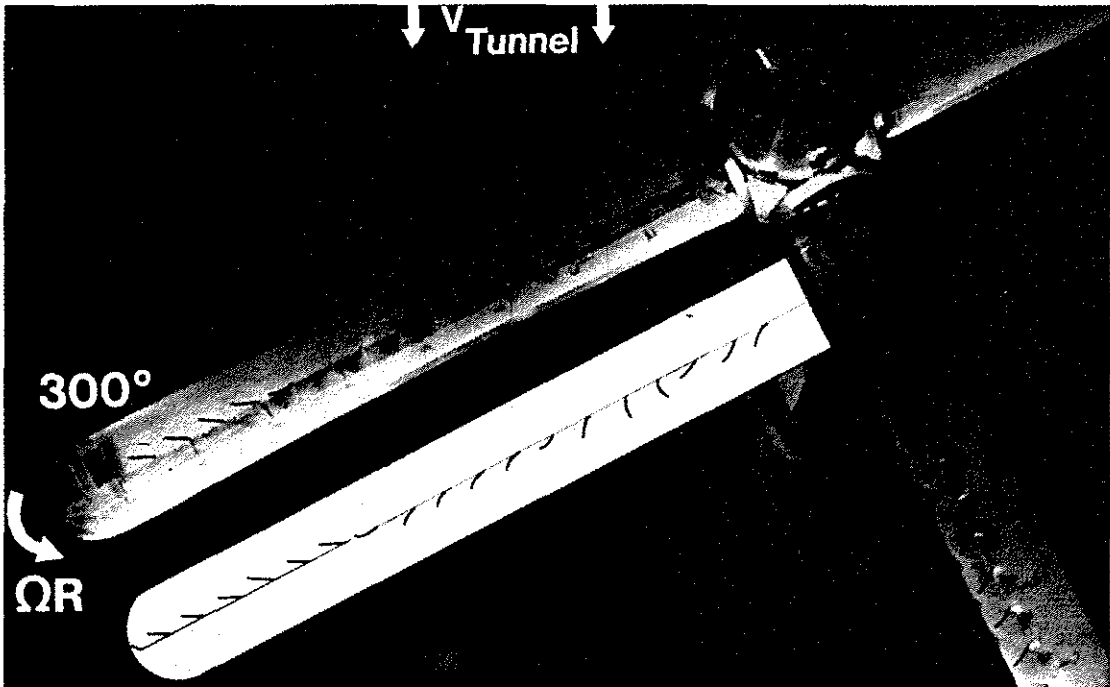


Figure 15 – Photograph of Fourth Quadrant, Conditions Same as in Preceding Figure

OBJECTIVES

- $\alpha - C_p$ CORRELATION
- UNSTEADY EFFECTS
- VORTEX INTERSECTIONS
- VORTEX INFLUENCES

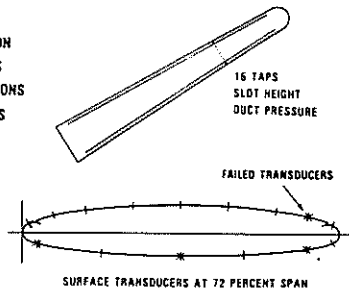


Figure 16 – Blade Section Aerodynamics (25-Foot-Rotor)

ADVANCE RATIO 0.4, AZIMUTH 18 DEG

TEST DATA UPPER (1) LOWER (1) SURFACE

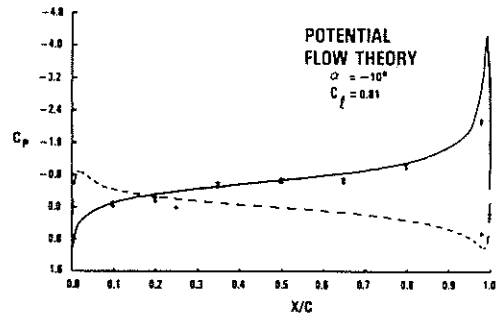


Figure 17 – Blade Section Surface Pressure Analysis

SPECTRUM ANALYSIS OF RBCCR MODEL

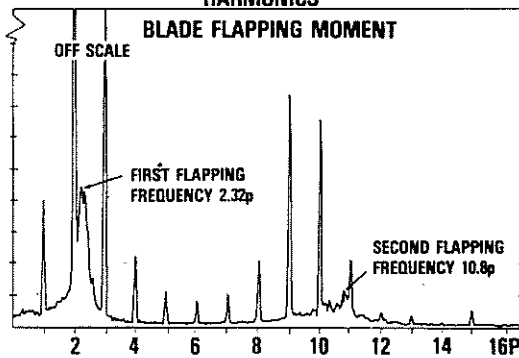
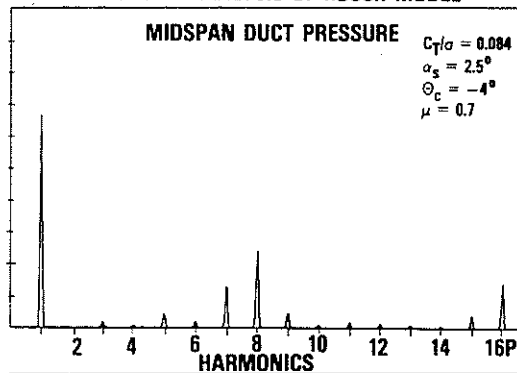


Figure 18 – Blade Flatwise Moment Response to Higher Harmonic (8p) Pressure Input (Reverse Blowing Circulation Control Rotor Data)

BENDING MOMENT WITH 1P PRESSURE WAVE

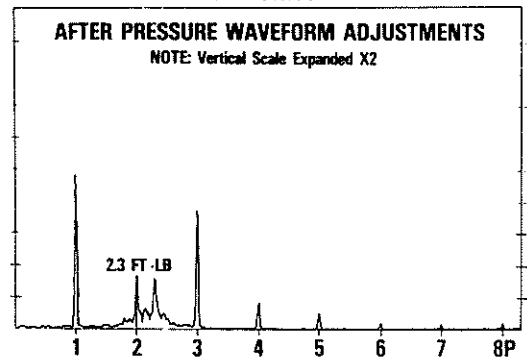
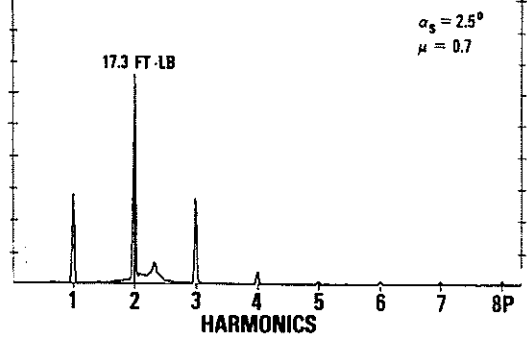


Figure 19 – Reduction of Blade 2p Flatwise Moment Through Control of Pressure Waveform (Experimental Results)

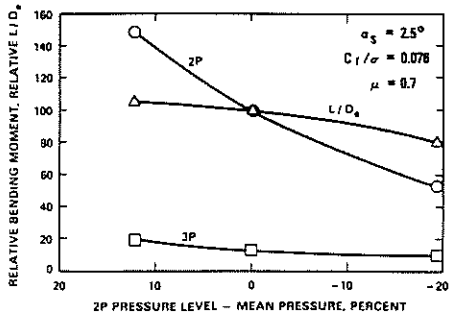


Figure 20 – Influence of Two-Per-Revolution Pressure Control Input (Experimental Data)

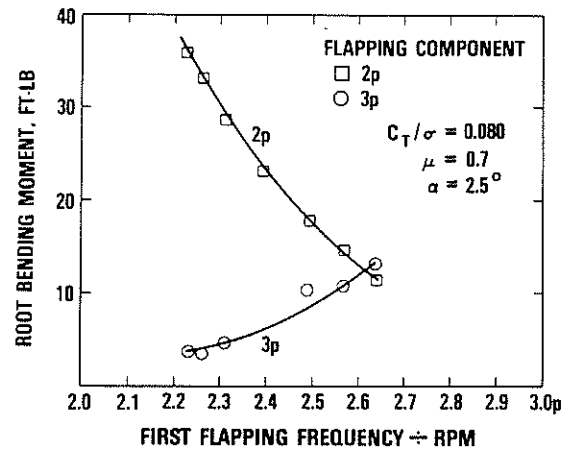


Figure 21 – Flapping Frequency Placement Investigation On Subscale Rotor (1p Control)

- TIP SPEED
- RADIUS
- TAPER
- SLOT HEIGHT
 - SPANWISE TAPER
 - FLEXIBILITY
 - OPENING PRESSURE
- AZIMUTH LOADING (WAVE FORM)
- DUAL VERSUS SINGLE BLOWING
- PRESSURE/MASS FLOW TRADEOFF
- SHAFT ANGLE
- CONVERSION SPEED
- FIXED/VARIABLE COLLECTIVE
- PEAK OPERATING PRESSURE
- AIRFOIL SELECTION
 - THICKNESS
 - CAMBER
 - SLOT POSITION
 - COANDA CONTOUR

TABLE 1 – Major Aerodynamic Design Parameters for High Speed Circulation Control Rotor

	LOADING SENSITIVE	VORTEX WAKE	INSTANTANEOUS V_i	VORTEX INTER-SECTION	COST TO USE	COMMENTS
UNIFORM MOMENTUM					LOW	'CONVENTIONAL'
DISTRIBUTED MOMENTUM	✓				LOW	LOCAL THRUST BALANCE
LINEAR VORTEX	✓	✓			MODERATE	USSR THEORY
FULL VORTEX	✓	✓	✓	✓	HIGH	RASA, INC. DEVELOPMENT

TABLE 2 – Major Features of Inflow Methods Investigated

DATA POINT 1122/371: $C_T/\sigma = 0.085$, $\alpha_s = 0$, ADVANCE RATIO = 0.7, +2p WAVE

	THRUST (LB)	ROLL (FT-LB)	PITCH (FT-LB)	TORQUE (FT-LB)	MASS FLOW (LB/SEC)
EXPERIMENT	64.3	2.3	-3.8	19.0	.601
UNIFORM MOMENTUM	82.6	57.2	-14.0	15.1	.619
DISTRIBUTED MOMENTUM	82.5	35.6	-2.9	17.4	.619
LINEAR VORTEX	83.1	14.3	-1	15.4	.619
FULL VORTEX	68.7	3.8	-3.6	24.6	.619

TABLE 3 – Experiment/Analysis Correlation as Function of Inflow Representation Utilized

NOTE: SINGLE SLOT THRUST IS 62 LB; TORQUE IS 14 FT-LB; $\mu = 0.7$

	Δ THRUST (LB)	Δ ROLL (FT-LB)	Δ PITCH (FT-LB)	Δ TORQUE (FT-LB)
EXPERIMENT	8.1	9.9	4.3	-4.4
THEORY	7.4	7.0	2.6	-3.0

TABLE 4 – Influence of Applying Dual Slot Blowing on the Retreating Side

$C_T/\sigma = 0.11$, $\alpha_s = 2.5^\circ$, $\mu = 0.7$

NOTE: 10 FT-LB = 4 PERCENT RADIUS THRUST OFFSET

	THRUST (LB)	ROLL (FT-LB)	PITCH (FT-LB)	TORQUE (FT-LB)
EXPERIMENT	84.5	-0.9	-1.0	13.3
DISTRIBUTED MOMENTUM	98.7	24.3	6.4	13.5
FULL VORTEX	86.3	1.5	-2.0	17.1

TABLE 5 – Correlation at High Thrust Level

NOTE: $C_T/\sigma = 0.089$, $\alpha_s = 0$, 1P CONTROL

	THRUST (LB)	ROLL (FT-LB)	PITCH (FT-LB)	TORQUE (FT-LB)
EXPERIMENT	69.4	0.5	-3.8	15.4
DISTRIBUTED MOMENTUM	83.9	37.2	-16.5	16.5
FULL VORTEX	72.7	6.7	-14.8	20.0

TABLE 6 – Additional Correlation Example

NOTE: $\alpha_s = 9$, $C_T/\sigma = 0.083$, 1P CONTROL

	THRUST (LB)	ROLL (FT-LB)	PITCH (FT-LB)	TORQUE (FT-LB)
EXPERIMENT	73.4	-2.9	-1.7	12.4
UNIFORM MOMENTUM	74.0	28.6	-10.3	11.0
DISTRIBUTED MOMENTUM	74.1	17.6	-10.3	12.7
FULL VORTEX	71.5	-3.0	-8.4	17.6

TABLE 7 – Correlation at Advance Ratio 0.30